Quest Journals
Journal of Architecture and Civil Engineering
Volume 4 ~ Issue 1 (2019) pp: 50-75
www.questjournals.org

Research Paper

Design, manufacture and simulation of Seismic Isolation Device for a Low Level Axial Load

Gustavo Gioacchini[1], Miguel Eduardo Tornello[1], Carlos Daniel Frau[1]
1 National Technological University, Mendoza Regional Faculty, CeReDeTeC
Corresponding Author: Gustavo Gioacchini

ABSTRACT:*Earthquakes are one of the natural phenomena that cause the greatest loss of human and economic lives yearly. Seismic-resistant structural engineering has developed new strategies to protect buildings from earthquakes such as seismic isolation. The records of the use of isolated structures indicate that seismic isolation has been used mainly to large undertaking, a highly positive situation and are used less frequently in many other widespread works such as one or two-story housing, commercial buildings and low-riseapartment buildings, structures and industrial equipment of low weight. The object of the present work is the design and manufacture of elastomeric devices for low axial load, even with their elastic and mechanical characterization. The isolation devices have two differences with those that are usually used worldwide. The first one is that they do not have intermediate steel plates vulcanized to the rubber layers and the second characteristic refers to the core of the device. The results of the experimental tests, of different prototypes, are presented to vertical and horizontal cyclic loads. Numerical models and their validation through experimental tests are also shown. The results indicate an acceptable behavior of the devices quantified in terms of damping and of the energy dissipated during the hysteretic cycles.*

KEYWORDS:*seismic isolation, manufacturing, experimental tests, numerical models, response simulation*

Received 08 Feb.., 2020; Accepted 24 Feb., 2020 © The Author(S) 2020.
Published with open access at Www.Questjournals.Org

I. INTRODUCTION

The seismic vulnerability inherent to the development of human activity should be minimized in every engineering work. The design of earthquakes resistant structures must comply with three basic premises, i) avoid the heavy loss of human life, ii) reduce public and private economic losses and iii) control the socio-economic delays caused by the occurrence of a destructive earthquake.

The behavior of structures subject to severe earthquakes has shown that the damage control philosophy is adequate in order to satisfy the first of all premises. The structures work in plastic range with non-recoverable damages. Therefore, the cost of the rehabilitation influences the premises to diminish the associated economic losses. During the 2000-2011 period, the direct economic losses associated with the earthquakes were US$ 536,319 million, which represents 40% of the total economic losses from natural disasters. [1].

The seismic isolation strategy is applied in seismic regions in order to protect important buildings or to fulfill essential functions after the earthquake. In fact, there are many examples in Europe, the United States, Japan, Italy and New Zealand. There are also projects of isolation housing actually built in Chile, Peru and the United States.

The strategy of seismic isolation has been oriented mainly to important works and infrastructure however, other massive construction works have been neglected (one or two-story housing, commercial buildings, hotels and low-rise apartment buildings, structures and industrial equipment, equipment of transforming stations, etc.) that, like great works, also suffer the impact of a destructive earthquake.

The purpose of this work is the development of a seismic isolation device with a low level of axial load. Seismic isolation devices with an elastomeric base have been designed and manufactured with characteristics different from those currently commercialized.There are some records of elastomeric isolation devices that use carbon fiber reinforcement plates to replace steel plates so as to reduce isolation costs. The use of carbon fiber allows to manufacture isolation in longitudinal strips which are really suitable for housing with concrete or masonry. Figure 1 shows a system of elastomeric isolation in longitudinal strips [2].

Another kind of isolation developed for lightweight constructions is made up of reinforced concrete connecting rods (PPP) [3]. The system was used in a housing in Chile. The housing is built on a floating slab

that rests on reinforced concrete connecting rod-like isolation and on two elastomeric isolation which function is to provide the restitutiva force. Figure 2 shows the finished housing and one of the reinforced concrete connecting bar which make up the isolation system (PPP) [4].The technique used the elastomeric isolation so as to guarantee the restitutiva force which increases costs and does not allow technological independence.

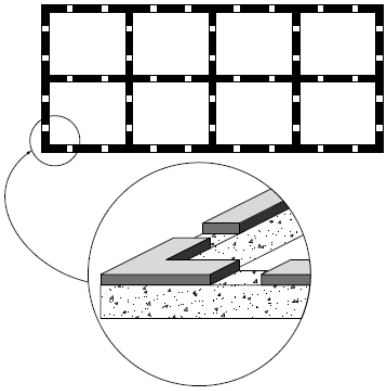

Figure 1. Elastomeric isolation in longitudinal strips [2].

In Ecuador, low cost elastomeric isolation devices have been built and tested to be used in housing. Good results have been obtained, but they have a low damping. In order to reduce the impact on the environment and costs, the devices were manufactured with recycled tire elastomers, Figure 3. [5] [6].

Figure 2. Housing with seismic isolation system PPP [4].

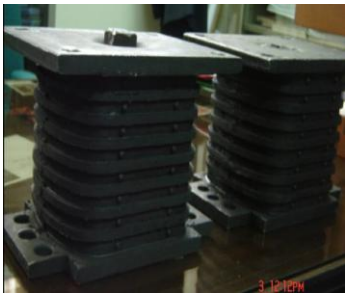

Figure 3. Devices manufactured in Ecuador with elastomers of disused tires.

Another record is the RBRL system, suggested by Prof. A.G. Thomas and developed in the Tun Abdul Razak Research Center (TARRC) to allow the isolation of low mass structures, for example, less than 10 tons [7]. The RBRL system comprises balls (usually made of steel) that roll on rubber layers joined to steel tracks with auxiliary quays of rubber decentering. These can be combined in individual packages as shown in Figure 4. The functions of the main components of the system are the following, i) system of rolling steel balls: it allows to support vertical loads; ii) rubber layer tracks: they provide energy dissipation and resistance for non-seismic horizontal actions and iii) rubber springs: they provide the function of recentering.

The records indicate few applications of the technique of seismic isolation in structures with low weight and that in addition, a new technology has been generated which allows to reduce the incidence of the devices in the final cost of the isolated structure.

*Corresponding Author:Gustavo Gioacchini51 | Page
National Technological University, Mendoza Regional Faculty, CeReDeTeC

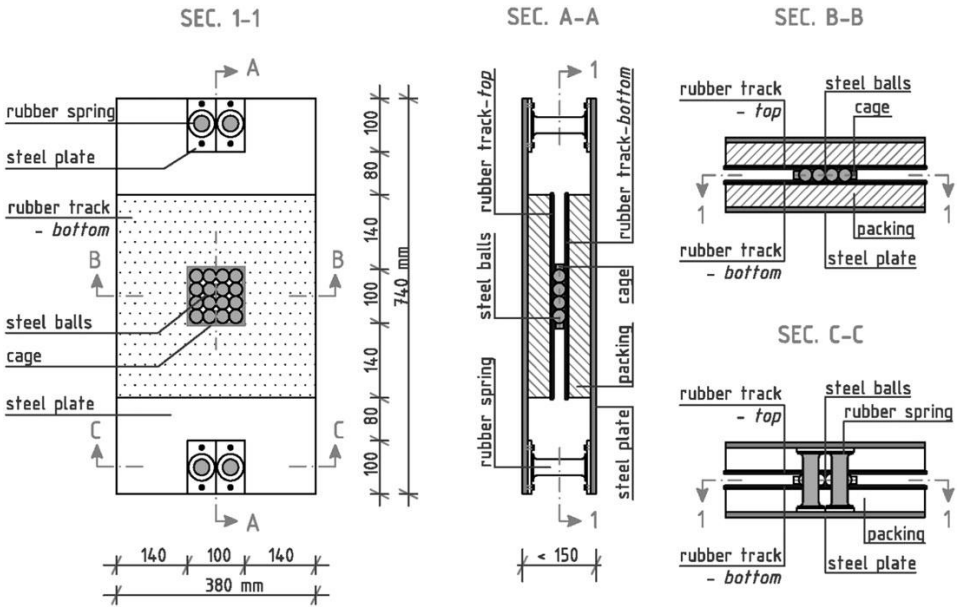

Figure 4. Scheme of the RBRL system [7].

II. DESIGN AND MANUFACTURE OF SEISMIC ISOLATION DEVICES

2.1. CHARACTERISTICS OF THEISOLATION AND THERUBBERCOMPOUNDUSED

The geometrical characteristics of the elastomeric isolation are shown in Figure 5. The device has two connecting steel plates, lower and upper, and a rubber blockof 200 mm of height and 180 mm of diameter.The isolation devices have two differences with those that are usually used worldwide. The first one is that they do not have intermediate steel plates vulcanized to the rubber layers. Therefore i) manufacturing costs are reduced, ii) the axial load capacity is reduced and iii) the effective rigidity of the devices is reduced. The second characteristic refers to the core of the device.

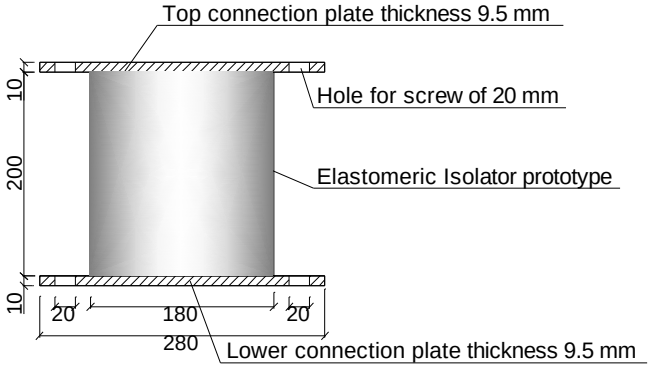

Figure 5. Characteristics of the isolation device (Dimensions in mm).

The devices that are used worldwide have, in some cases, lead cores while those developed in the present work have an elastomer core confined to a steel tube or with sheets of fibers (cord fabric). This characteristic allows a reduction in manufacturing costs and allows a new technological development in the country.

The base compound for the manufacture of isolation are the following [8]: Hardness: 60 +/- 10 shore; Maximum stress> 17 MPa; Maximum elongation> 400%; Damping> 8%; Cutting module: 0.70 <G <0.8 MPa. The components and their proportions are summarized in Table 1 [9].

*Corresponding Author:Gustavo Gioacchini52 | Page
National Technological University, Mendoza Regional Faculty, CeReDeTeC

Table 1. Components of the rubber compound

Rubbercomponents 8654			
Componentsfor 1kg		Characteristics – Properties	Quantity [kg]
Elastomer	Neoprene W	Base elastomer	0,293
	Caucho Natural		0,245
Loads	Smoke Black FEF	Black load highly reinforcing of physical properties	0,234
	SilicePrecipitated		0,088
AuxiliariesofProcess		Vulcanizationsystemactivators	0,033
Activators		Activantes del sistema de vulcanización	0,065
Antioxidants and Antiozonates		They are used as protectors of degradation by oxidation and heat	0,027
Catalysts and Retardants		Exerts retarding properties during vulcanization	0,015

2.2. TESTSONRUBBERCOMPOUNDS

In order to determine the mechanical properties of the compounds, the following tests have been carried out:

2.2.1. HARDNESS

The hardness of the compounds was determined according to IRAM 11303 and ASTM D2240 [10] [11]. The test consists of the penetration of a normalized indenter in the material. The indentation hardness is inversely proportional to the penetration and depends on the module of elasticity and the viscoelastic behavior of the material.The test was performed on a test tube composed of a sheet of circular section of 80 mm of diameter with a thickness of 13.08 mm. The hardness obtained in the test for the rubber compound used in the manufacture of the isolation devices was of 65 shore. This value is within the acceptable ranges for compounds used in the manufacture of elastomeric isolation.

2.2.2. TEST OF RESISTANCETOMAXIMUM STRESS AND BREAK ELONGATION

The tests were performed according to ASTM D412 [12]. The method allows to measure the strain properties of a rubber compound at different temperatures. The strain properties of the rubber depend on the material and the test conditions, such as speed, temperature, humidity and geometry of the test tube. In Table 2 shows the data obtained for the series of tests.

Table 2. Results of traction and elongation tests of the elastomer.

TRACTION AND ELONGATION TESTS						
Specimens	Thickness mm	Width mm	Area (A) mm^2	Force (F) N	Tension (s) MPa	Elongation %
1	1,8	7	12,6	240	19,05	440
2	1,78	7	12,46	205	16,45	395
3	1,83	7	12,81	215	16,78	405
4	1,7	7	11,9	210	17,65	430
Average					17,48	418

2.2.3. RESIDUAL COMPRESSION TEST

The tests are based on the ASTM-D395 standard [13]. The purpose of the test is to measure the capacity of the rubber compound in order to retain its elastic properties after an extended compression. It is made in rubber that may be exposed to compression stress in the air or in liquid media. The result is obtained with the following expression:

$$R_{ec} = \frac{T_0 - T_f}{T_0 - T_s} * 100 \qquad \rightarrow 1$$

Where: T_0= Initial thickness of the test tube.
T_f = Final thickness of the test tube
T_s = Height of the spacer, (25%).

*Corresponding Author:Gustavo Gioacchini53 | Page
National Technological University, Mendoza Regional Faculty, CeReDeTeC

The final measured thickness of the test tube (Tf) was of 12.48 mm. Therefore, the residual compression was:

$$R_{ec} = \frac{T_0 - T_f}{T_0 - T_s} * 100 = \frac{13{,}08mm - 12{,}48mm}{13{,}08mm - 9{,}5mm} * 100 = 16{,}76$$

2.3. MANUFACTURE OF SEISMICISOLATIONDEVICES

The molds used in the manufacture are made of solid steel and were specially built. They consist of an inner tube with a wall thickness of 54 mm, sectioned in the middle in order to allow unmold, and an external tube of 30 mm thick to keep the inner parts together during the manufacturing devices (Figures 6 and 7).

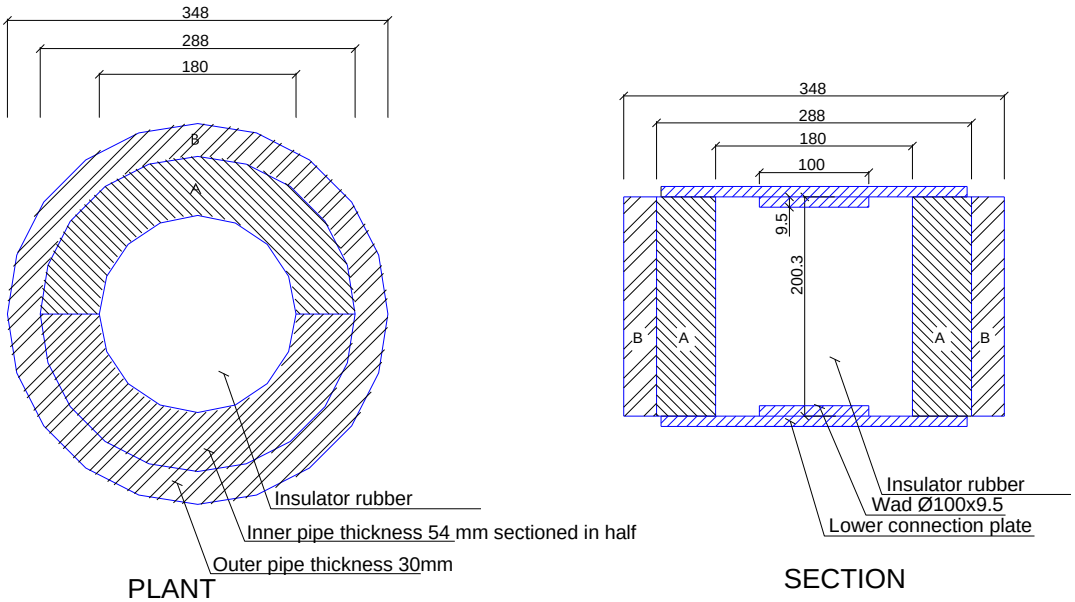

Figure 6. Molds used in the manufacturing of seismic isolation devices

Figure 7. Molds used in the manufacturing of the seismic isolation devices

The lower and upper connection plates have 9.5 mm of thickness and 280 mm of a diameter. They have a steel plug in the center of 100 mm of diameter and 9.5 mm of thickness which function is to provide a greater contact surface with the elastomer. Four holes for bolts of 20 mm have been designed to allow connection with the foundation structure and the superstructure. In order to facilitate its positioning, a steel ring with three bolts has beenmade, to thread the ears attached to the mold. The connection plates and the centering ring are shown in Figures 8, 9 and 10.

*Corresponding Author:Gustavo Gioacchini54 | Page
National Technological University, Mendoza Regional Faculty, CeReDeTeC

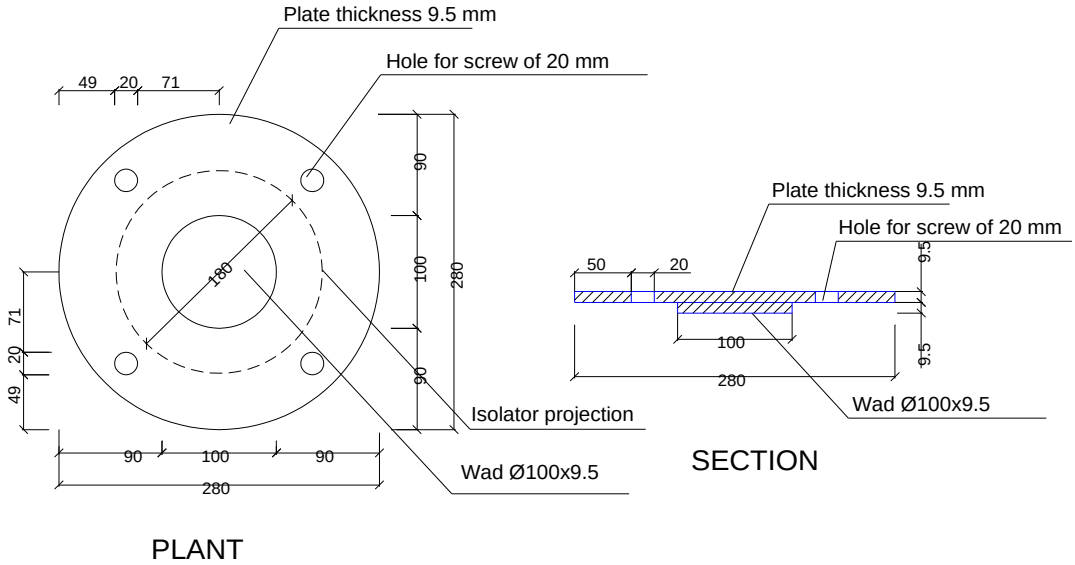

Figure 8. Lower and upper connection plates of seismic isolation device.

Eight devices have been manufactured with four types of core confinement. The first series of isolation (two prototypes) have been manufactured without a confining core (ASND). The second series (two prototypes) have confined cores with a grooved steel tube of 100 mm of diameter and 6 mm of thickness (ANAG) and the third series (two prototypes) have a confined core with fiber sheets (cloth cord) of 100 mm of diameter (ANTC).

The fourth series (two prototypes) have a confined core with a perforated sheet steel tube 100 mm of diameter and 2 mm of thickness (ANAF). In all cases the confined core does not interest the entire height of device. They have a height of 110 mm with a separation of 45 mm with the upper and lower connection plates. In Figure 11 the cores placed in the second and third series are shown.

Figure 9. Connection plates and the centering ring.

Figure 10. Molds, connection plates and centering ring.

*Corresponding Author:Gustavo Gioacchini55 | Page
National Technological University, Mendoza Regional Faculty, CeReDeTeC

Figure 11. Cores of the (ANAG) and (ANAF) prototypes.

The base material has been placed manually and the components were mixed mechanically. A non-adhesive additive has been applied to the inner part of the mold to facilitate its removal from the mold. The connection plates are painted with a special adhesive in order to improve the adhesion with the elastomer. The vulcanization consists of subjecting the rubber compound to a pressure of 120 tons and a temperature of 150ºC for a period of two hours. The pressure, temperature and time depend on the dimensions of the device. When they are removed from the press, they are cooled and the test tube is removed from the mold. Figures 12 show the devices at the time of vulcanization and Figure 13 shows the devices removed from the mold.

Figure 12. Devices prior to vulcanizing process. Vulcanizing process and positioning of the upper connection plate and final vulcanization.

Figure 13. Removing the seismic isolation devices.

*Corresponding Author:Gustavo Gioacchini56 | Page
National Technological University, Mendoza Regional Faculty, CeReDeTeC

III. EXPERIMENTAL ANALYSIS

3.1. TESTSONVERTICAL LOADS

3.1.1. TEST DESCRIPTION

Tests have been carried out to control vertical axial load on a universal machine, Shimadzu brand, with a loading capacity of 1000 KN.The tests have been carried out under controlled vertical deformation. For ASND and ANTC devices it has been deformed up to 50 mm. For the ANAG devices, the deformation has been 15 mm and for the ANAG devices, the deformation has been 100 mm. In all cases with the exception of the ANAF, the deformation has not exceeded the elastic range. Therefore,all device recovered their initial shape once the axial load was removed. The ANAF devices remained moderate permanent deformations. For the ANAG devices, the deformations have been defined so that the extremeplates did not contact the confinement core. For the ANAF devices, a deformation of 100 mm has been applied in order to achieve a level of permanent deformations. For the rest of the devices, the controlled deformation has been defined so as not to exceed 25% of the height of the isolation. In Figure 14, the tests to vertical axial loads are shown.

Figure 14. Test on vertical axial load of the ASND device.

3.1.2. RESULTS

Figure 15 shows the relationship force-displacement for the four devices tested. The ANAG-1 device has the highest vertical rigidity. By comparing the ASNC-1 device and the ANTC-1, it is observed that for the same displacement a vertical force is obtained in the ANTC-1, 1.6 times greater. If we compare it with the ANAF-1, the vertical force is 1.7 times greater.

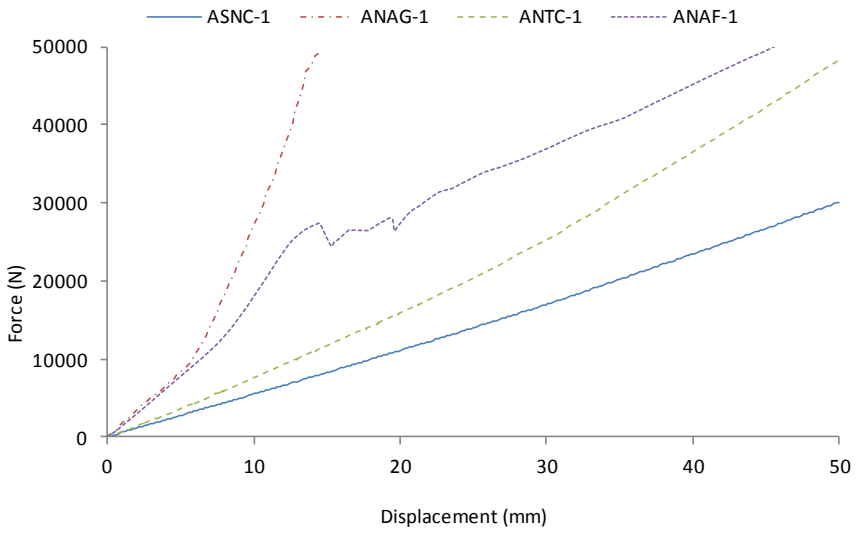

Figure 15. Relationship Force-displacement superimposed for the four prototypes.

The vertical rigidity of each device is obtained from the experimental tests to vertical loads. The ASNC, ANTC and ANAF devices show an almost constant rigidity during the whole test. The ANAG devices show a variation of the rigidity during the test. For this reason, the ANAG devices are characterized by an initial vertical rigidity and a final vertical rigidity.With equation (2) the vertical rigidity of the ASNC device is determined.

*Corresponding Author:Gustavo Gioacchini57 | Page
National Technological University, Mendoza Regional Faculty, CeReDeTeC

Vertical rigidity: $K_v = \frac{|F^+|}{|\Delta^+|} = 602\,{}^{N}\!/_{mm}$ → 2

F^+= 30.100 N Δ^+= 50 mm

Table 3 summarizes the values obtained from the experimental tests. Where△+ y F+are the displacement and the maximum force.

Table 3. Vertical rigidity of the seismic isolation devices.

Parameter	Unit	PROTOTYPES OF ISOLATORS				
		ASNC-1	ANAG-1		ANTC-1	ANAF-1
			Initial	Final		
F^+	N	30.000	8.180	49.500	50.700	51.640
Δ^+	mm	50,00	4,90	14,50	51,74	47,41
k_v	N/mm	600,05	1.669,39	3.413,79	979,98	1.089,18

3.2. TESTING OF DEVICESTOCONSTANT VERTICALLOADS AND CYCLICAL HORIZONTAL LOADS

3.2.1. TEST DESCRIPTION

Tests have been carried out with a steel frame. A 12 ton hydraulic actuator to apply the cyclic horizontal load and four threaded rods fixed to the reactive slab to apply the vertical load. The diagram of the test is shown in Figure 16.The digital data acquisition system consists of sensors, measurement hardware and a PC with programmable software in real time. The sensors are load cells to measure the vertical loads, a load cell to measure horizontal forces, a linear variation differential transformer (LVDT) to measure horizontal displacements and three potentiometers to measure the vertical displacements.

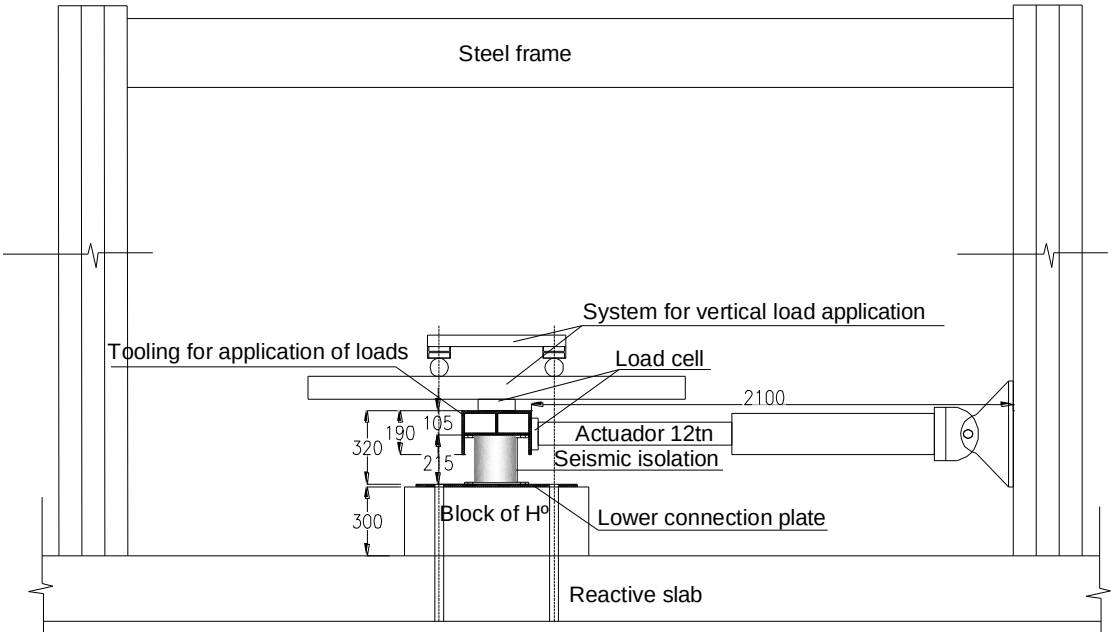

Figure 16. Diagram of the device test.

The devices have been tested for two vertical displacements, 15mm and 30mm. For each vertical displacement, seven cycles of horizontal displacements of +/- 10 mm, 20 mm, 30 mm, 40 mm, 50 mm, 60 mm and 70 mm have been made. Figure 17 shows the testing of one of the devices.

*Corresponding Author:Gustavo Gioacchini58 | Page
National Technological University, Mendoza Regional Faculty, CeReDeTeC

Figure 17. Experimental tests of prototypes

3.2.2. RESULTS

The following parameters were determined from the experimental results: i) the relationship force-displacement. Hysteresis curve; ii) hysteretic loops, average area and energy dissipated by the device and iii) the maximum forces and displacements to determine the effective rigidity.Figure 18 shows the horizontal relationshipforce-displacement of the ASNC-1 device for vertical displacement of 15mm and vertical load of 8,000 Nand Figure19 shows the horizontal relationship force-displacement of the ASNC-1 devicefor vertical displacement of 30mm and vertical load of 17,000 N.

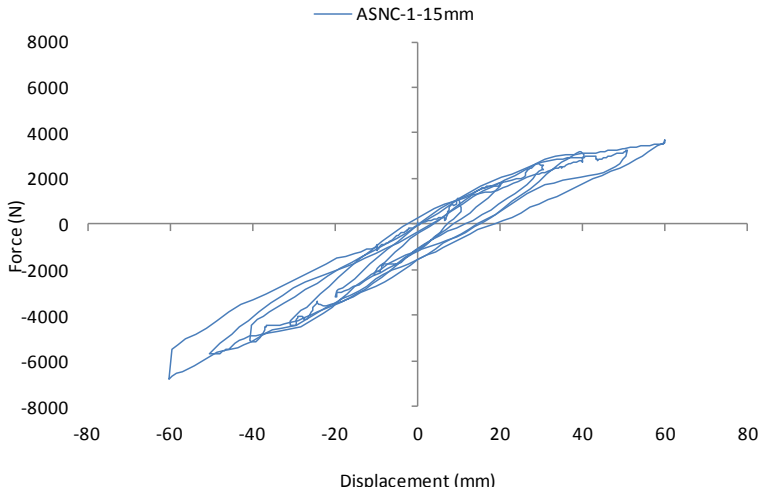

Figure 18. Relationship force-displacement for the ASNC-1-15mm device

Figure 19 shows the horizontal relationship force-displacement of the ASNC-1 device, for two vertical displacements (15mm and 30mm). Figure 20 shows the horizontal relationship force-displacement of the ANAG-1 device for vertical displacement 15mm and vertical load of 20,200 N. Figure 21 shows the horizontal relationship force-displacement of the ANAG-1 device for vertical displacement of 3 mm and vertical load of 4,000 N and Figure 22 shows the horizontal relationship force-displacement of the ANAG-1 device for two vertical displacements (15mm and 3mm).

*Corresponding Author:Gustavo Gioacchini59 | Page
National Technological University, Mendoza Regional Faculty, CeReDeTeC

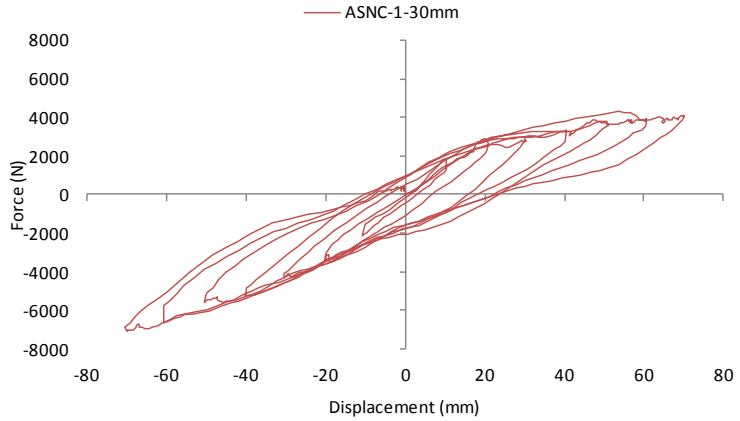

Figure 19. Relationship force-displacement of the ASNC-1-30mm device.

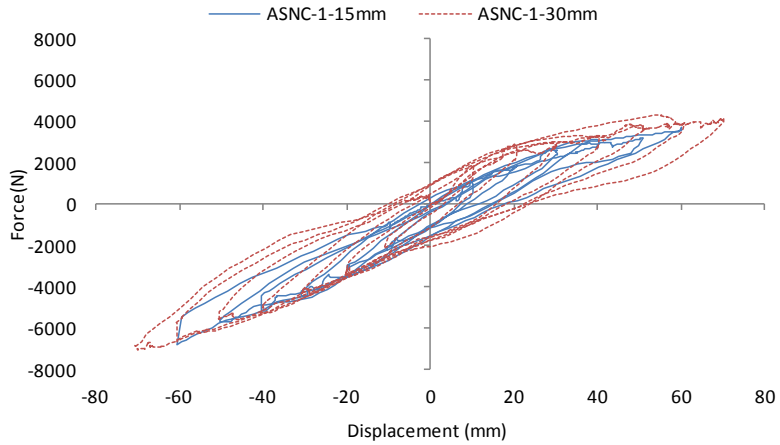

Figure 20. Relationship force-displacement for the ASNC-1 device for vertical displacements of 15mm and 30mm.

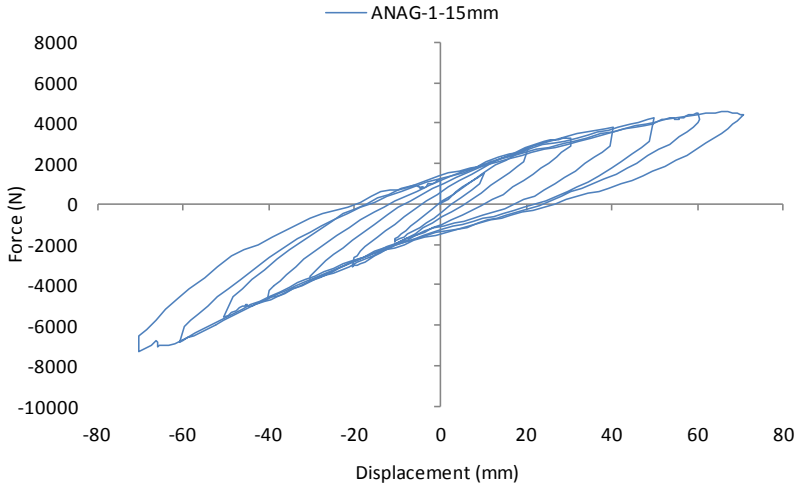

Figure 21. Relationship force-displacement for the ANAG-1-15mm device.

*Corresponding Author:Gustavo Gioacchini60 | Page
National Technological University, Mendoza Regional Faculty, CeReDeTeC

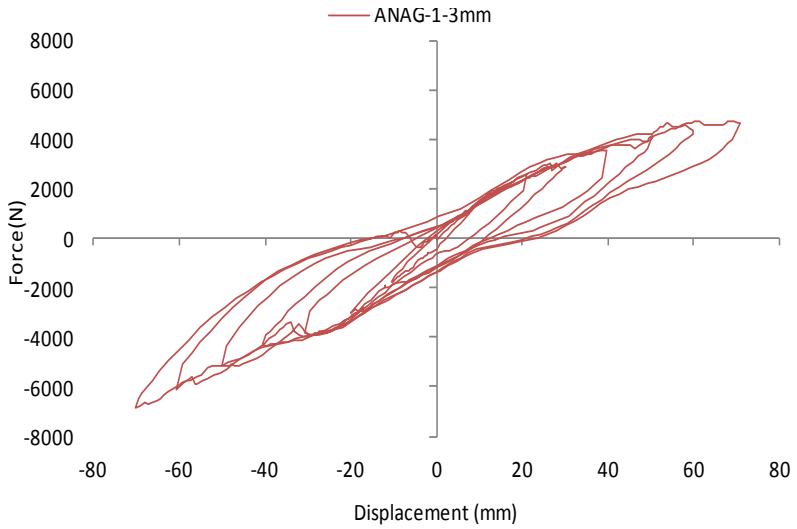

Figure 22. Relationship force-displacement of the ANAG-1-3mm device.

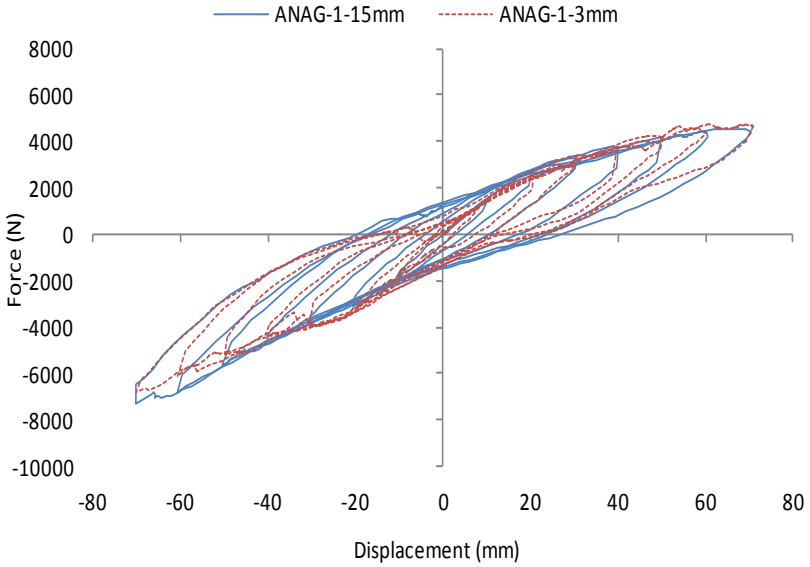

Figure 23. Relationship force-displacement of the ANAG-1 device, for vertical displacements of 15mm and 3mm.

Figure 24 shows the horizontal relationship force-displacement of the ANTC-1 device for vertical displacement of 15mm and vertical load of 9,000 N. Figure 25 shows the horizontal relationship force-displacement of the ANTC-1 device for vertical displacement of 30mm and vertical load of 18,000 N and Figure 26 shows the horizontal relationship force-displacement of the ANTC-1 device for the two vertical displacements (15mm and 30mm).

Finally, Figure 27 shows the horizontal relationship force-displacement of the ANAF-1 device for vertical displacement of 15mm and vertical load of 20,200 N.

*Corresponding Author:Gustavo Gioacchini61 | Page
National Technological University, Mendoza Regional Faculty, CeReDeTeC

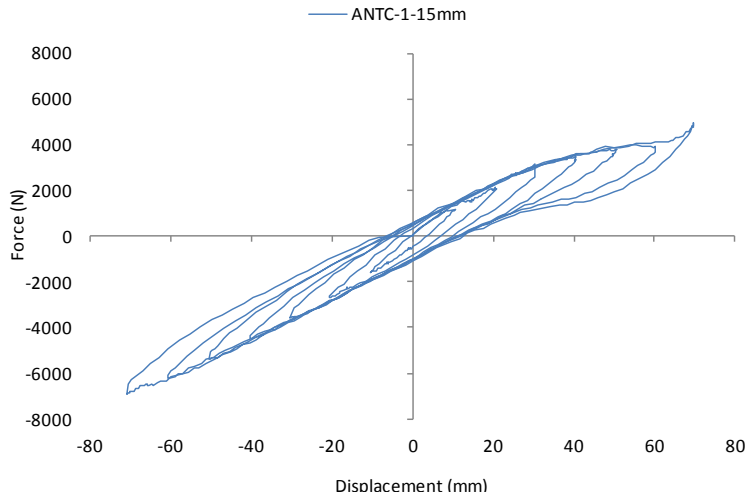

Figure 24. Relationship force-displacement of the ANTC-1-15mm device.

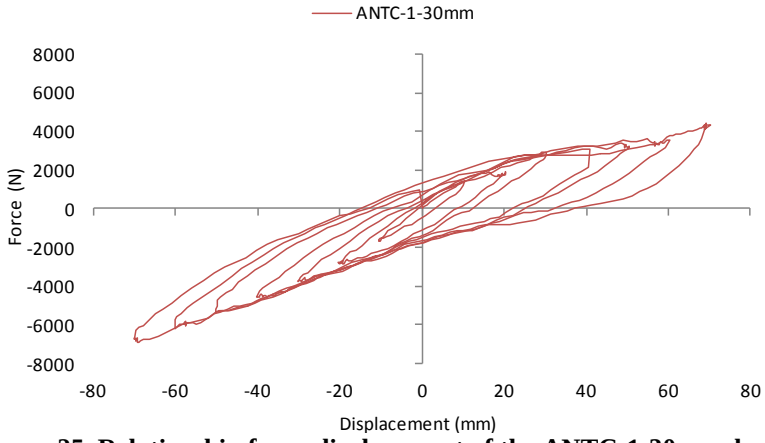

Figure 25. Relationship force-displacement of the ANTC-1-30mm device.

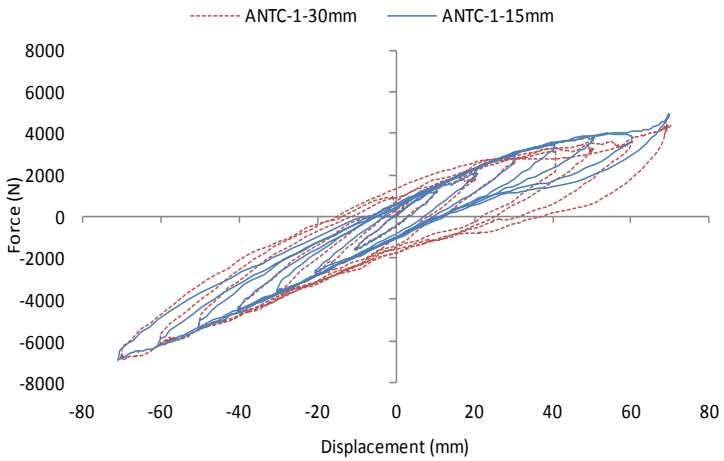

Figure 26. Relationship force-displacement for the ANTC-1 device, for vertical displacements of 15mm and 30mm.

*Corresponding Author:Gustavo Gioacchini62 | Page
National Technological University, Mendoza Regional Faculty, CeReDeTeC

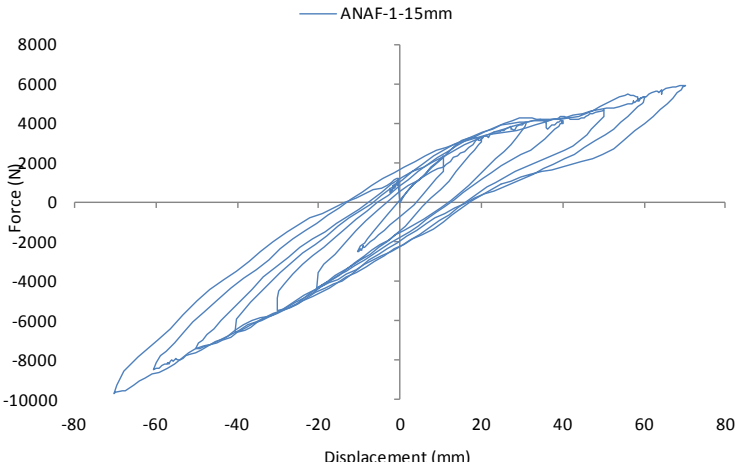

Figure 27. Relationship force-displacement for the ANAF-1-15mm device.

The result show, when vertical displacements increase, the horizontal forces-displacements curves enclose larger areas. The effective horizontal rigidity of the devices does not show a significant degradation when the vertical load and the horizontal force are increased. The effective rigidity of the devices remains almost constant throughout the entire test and for the imposed load stages. The response of the devices shows a noticeable non-linearity in the loading and unloading cycles.Table 4 summarizes the characteristic parameters of the devices obtained from the tests.

Table 4. Characteristic parameters of the devices obtained from the experimental tests.

Para-meter	Unit	PROTOTYPES OF ISOLATORS										
		ASNC-1		ASNC-2		ANAG-1		ANAG-2	ANTC-1		ANTC-2	ANAF-1
		15 mm	30 mm	15 mm	30 mm	15 mm	30 mm	15 mm	15 mm	30 mm	15 mm	15 mm
F_y	N	1.654	1.640	1.545	1.614	1.577	1.415	1.580	1.420	1.480	1.550	1.685
D_y	mm	10,33	9,80	9,36	9,80	10,35	9,90	8,50	10,10	10,30	10,75	11,90
K_u	N/mm	160,05	167,35	165,06	164,69	152,37	142,93	185,88	140,59	143,69	144,19	141,60

3.2.3. RIGIDITY AND EFFECTIVEDAMPING

Of the experimental result, the rigidity and effective damping [14] of the devices was determined. The procedure for a case is described and the rest of the results are summarized in Table 5. Figure 28 shows the area of the surrounding hysteretic cycle of the ASNC-1-15mm prototype.

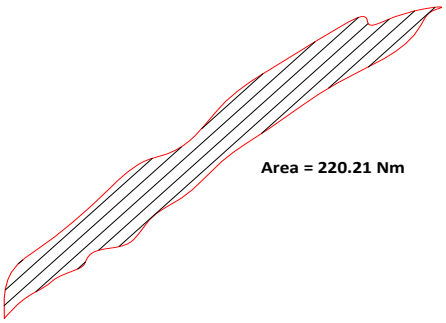

Figure 28. Area of the surrounding hysteretic cycle of the ASNC-1-15mm device.

The harmonic linearization is applied in order to determine the energy dissipated by a linear system and other parameters that characterize each type of device. [14]

Effective rigidity: $$K_{eff} = \frac{|F^+| + |F^-|}{|\Delta^+| + |\Delta^-|} = 87{,}64\ {}^{N}\!/_{mm} \qquad \rightarrow 3$$

F^+= 3.709 NΔ^+= 60 mmF^-= -6.808NΔ^-= -60 mm
W_o = Hysteretic cycle area= 220.210 Nmm

*Corresponding Author:Gustavo Gioacchini63 | Page
National Technological University, Mendoza Regional Faculty, CeReDeTeC

Elastic energy: $$w_e = \frac{1}{2} K_{eff} \delta^2 = 157.755 Nmm \rightarrow 4$$

Effective damping: $$\xi_{eff} = \frac{w_0}{4\ \pi\ w_e} = \frac{220.210 Nmm}{4\ \pi\ 157.755 Nmm} = 0{,}111 = 11{,}1\% \rightarrow 5$$

Table 5 summarizes the results of rigidity and the effective damping of all devices. Where $W_o$is the hysteretic cycle area; $F+$ and $F-$ are the maximum and minimum forces obtained from the hysteretic cycle;Δ^+y Δ^- are the maximum and minimum displacements obtained from the hysteretic cycle;$k_{eff}$is the effective rigidity andW_e is elastic energy.

Table 5. Effective rigidity and damping of the devices.

Parameter	Unit	PROTOTYPES OF ISOLATORS										
		ASNC-1		ASNC-2		ANAG-1		ANAG-2	ANTC-1		ANTC-2	ANAF-1
		15 mm	30 mm	15 mm	30 mm	15 mm	3mm	15 mm	15 mm	30 mm	15 mm	15 mm
W_o	Nmm	220.21	400.13	315.59	442.02	406.18	361.33	588.49	261.48	395.29	327.50	434.65
F^+	N	3.709	4.000	5.481	4.759	4.554	4.736	5.923	4.926	4.365	4.863	5.901
F^-	N	6.808	6.865	7.236	7.616	7.348	6.836	6.665	6.928	6.793	7.104	9.730
Δ^+	mm	60,00	70,00	71,00	70,00	70,00	71,00	71,00	70,00	70,00	71,00	70,00
Δ^-	mm	60,00	71,00	70,00	70,00	70,00	70,00	70,00	71,00	70,00	70,00	70,00
k_{eff}	N/mm	87,64	77,06	90,19	88,39	85,01	82,07	89,28	84,07	79,70	84,87	111,65
W_e	Nmm	157.755	188.789	227.328	216.563	208.285	206.860	225.022	205.974	195.265	213.921	273.543
ξ_{eff}	%	11,11	16,87	11,05	16,24	15,52	13,90	20,81	10,10	16,11	12,18	12,64

The results indicate that the effective damping has acceptable values (10% to 20%) and similar to conventional elastomeric isolation. It is observed for all devices, that the greater the vertical displacement is (greater axial load), the greater the effective damping will be, and so is the dissipation of energy.

IV. NUMERICAL MODEL SIMULATION

4.1. OBJETIVE

In order to validate the numerical models that correspond to the results of the devices tests, the mechanical response is studied numerically, considering the non-linear behavior of the component materials and the interaction between them as from a combination of imposed loads. Two methodologies have been used.

The first onewas Bouc-Wen model (point 4.2) with which the constitutive model of the isolation is represented and is compared to that obtained from the experimental tests. For this reason, the MatLab commercial platform is used [15].In the second methodology, the response of the device is numerically studied using the Ogden hyper elastic model (point 4.3). In order to do this, the device is shaped in finite elements with the Abaqus commercial code [16).

4.2. SIMULATION WITH BOUC-WEN MODEL

Wen model [17] [18] [19] has been used to represent the response of the device on a non-linear basis. The model decomposes the elastoplastic response into a component proportional to the displacement and another one dependent on a *z* variable. The restoration force *f*, is defined by expression (6):

$$f = \alpha\ k_i q_b + (1-\alpha) k_i z \rightarrow 6$$

Where $\alpha = k_j / k_i$ is a parameter that indicates the degree of non-linearity of the system (for example α = 1 represents a linear system) and z is a hysteretic parameter that satisfies the first-order non-linear differential equation [17] [18] [19]:

$$z = A\ q_b - \left(\beta\ q_b |z|^n + \gamma |q_b|\ |z|^{n-1} z \right) \rightarrow 7$$

The parameters *A, α, β, γ, n,* of the equations (6 and 7) are dimensionless numbers and regulate each one of the characteristics of the model behavior. Therefore, they represent the different types of non-linear behaviors [17] [18] [19]. The meaning of the parameters is:

*Corresponding Author:Gustavo Gioacchini64 | Page
National Technological University, Mendoza Regional Faculty, CeReDeTeC

A: General scale factor;
α: Reason between pre and post-creep rigidity;
β, *γ*: They determine the shape of the curve;
n: It regulates the smoothness of the transition between the linear and non-linear regions;
q_b: creep displacement.

The influence that the parameters *β* and *γ* have on the z variable can be visualized in the graph of the variable versus the displacement, for an external request of a periodic type (sinusoidal through time) that affects an oscillator of a degree of freedom and in which the restorer force represented by the Bouc-Wen model is included. [18]. For example, Figure 29 shows the hysteretic behavior represented by the parameters β = 0.5 and γ = 0.5

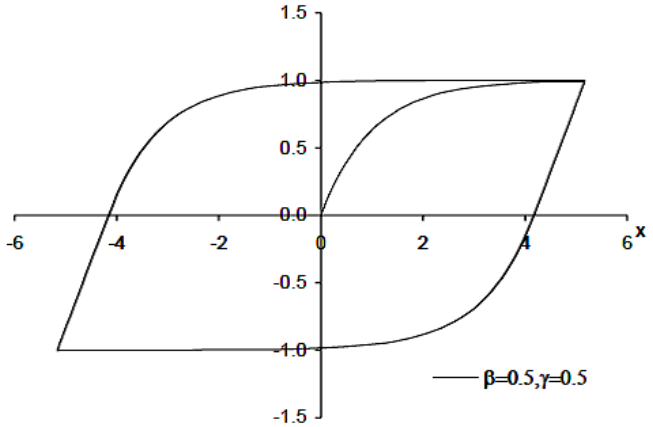

Figure 29. Hysterical curve of *z* versus x with β = 0.5 and γ = 0.5.

The parameter *n* has a range of variation between [1, + ∞] and controls the smoothness of the curves between the pre- and post-creep region. The higherthe value used, the greater is the transition curve and the Z value takes a value very close to 1 (Figure 30) [18] [19]. In order to completely eliminate the curved portion and thereby represent the bilinear model, the value of n → + ∞. It has been observed through practice that it is enough to take values of n of the order of 50 to obtain the representation of the bilinear model [20].

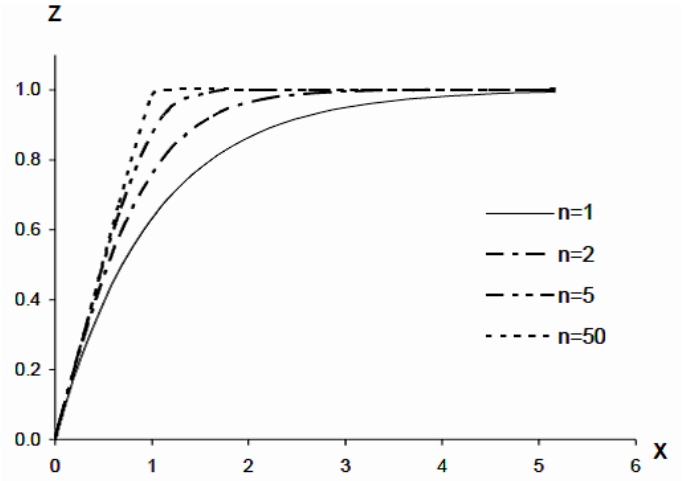

Figure 30. Behavior of the z variable with A= 1, α= 0.6, β=γ= 0.5, and different values of n.

The frequent parameters used for the modeling of elastomeric-type isolation are, A=1, β=- 0.54 and γ = 1.4. [17] For most authors, the most representative value to estimate the transition curve is n = 1, although in the SAP2000 and ETABS programs, a bidirectional variation of the model is used, which is equivalent to theformula of Bouc-Wen with n = 2 [20]. The SAP2000 and ETABS Programs have the Wen model incorporated as a non-linear element through the following equivalence relations [20]:
The non-linear force-deformation relationship or restorer force is:

$$f = r\,k_i d + (1-r) f_y z \rightarrow 8$$

Where: *ki*: Initial rigidity; d: Deformation;*fy*: Creep force; *r:* Creep radio (is the relationship between the post-creep rigidity and the initial rigidity*ki*); *z:* hysteretic variable, with variation interval of -1≤ z ≤1, the initial value of *z* is zero and z responds to the following differential equation:

$$z = \frac{k_i}{f_y} \begin{cases} d\left(1 - |z|^e\right) \Rightarrow d_z > 0 \\ d \Rightarrow d_z < 0 \rightarrow 9 \end{cases}$$

Where *e* is a transition parameter from the elastic to the inelastic phase (equal to n). Equation 9 is equivalent to the Bouc-Wen model for A = 1, β = 0.5 and γ = 0.5 (Figure 29).

4.2.1. CALIBRATIONOF BOUC-WEN MODELPARAMETERS

In order to calibrate the parameters of the Bouc-Wen numerical model, the commercial code MatLab is used. The influence of the parameters in the response has been controlled by an external vibratory input over time. The rest of the parameters used in the MatLab routine have been those obtained from the tests to vertical and horizontal cyclic loads.Table 6 shows the parameters corresponding to the Wen model that have been used in the numerical calibration of each device tested.

Table 6. Parameters corresponding to Bouc-Wen model.

Parameter	Units	PROTOTYPES OF ISOLATORS										
		ASNC-1		ASNC-2		ANAG-1		ANAG-2	ANTC-1		ANTC-2	ANAF-1
		15 mm	30 mm	15 mm	30 mm	15 mm	3 mm	15 mm	15 mm	30 mm	15 mm	15 mm
F_{vert}	N	49.050	49.050	49.050	49.050	49.050	49.050	49.050	49.050	49.050	49.050	49.050
m	kg	5.000	5.000	5.000	5.000	5.000	5.000	5.000	5.000	5.000	5.000	5.000
k	N/mm	600	600	600	600	600	600	600	600	600	600	600
F_y	N	2.600	2.600	2.700	2.600	2.600	2.600	2.700	2.600	2.700	2.600	2.600
X_y	mm	34,00	37,00	38,00	35,00	37,00	35,00	37,00	36,00	37,00	36,00	40,00
α		0,50	0,50	0,50	0,50	0,50	0,50	0,50	0,50	0,50	0,50	0,50
β		0,12	0,13	0,11	0,14	0,13	0,14	0,16	0,11	0,13	0,11	0,13
γ		0,88	0,87	0,89	0,86	0,87	0,86	0,84	0,89	0,87	0,89	0,87

4.2.2. RESULTS OF CALIBRATION

In order to evaluate the degree of approximation, the hysteretic cycles of Bouc-Wen model are compared to those obtained in the experimental tests. It is hereby stated that the hysteretic cycles of the experimental tests do not present symmetries due to the one used in the tests, while the cycles obtained with the Bounc-Wen model are symmetrical and have softer curves. The hysteretic cycles of the test and those obtained with the Wen model for some of the devices are superimposed in the following Figures.

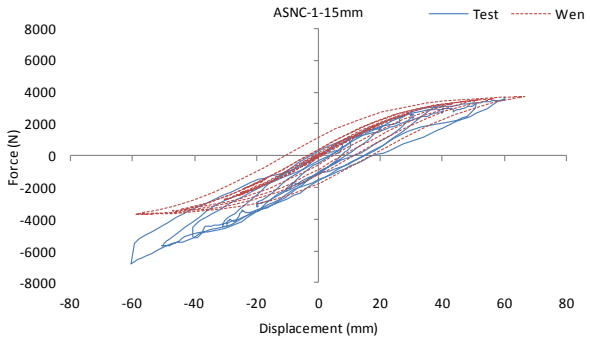

Figure 31. Comparison of the hysteretic cycles of the experimental test with those of the Bouc-Wen model for the ASNC-1-15mm device

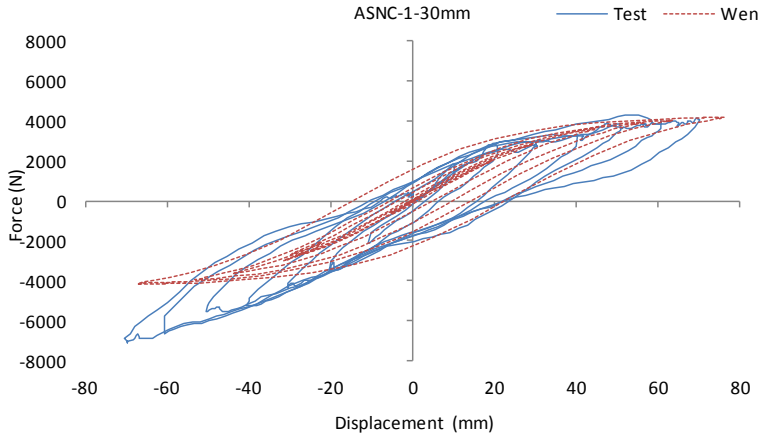

Figure 32. Comparison of the hysteretic cycles of the experimental test with those of the Bouc-Wen model for the ASNC-1-30mm device.

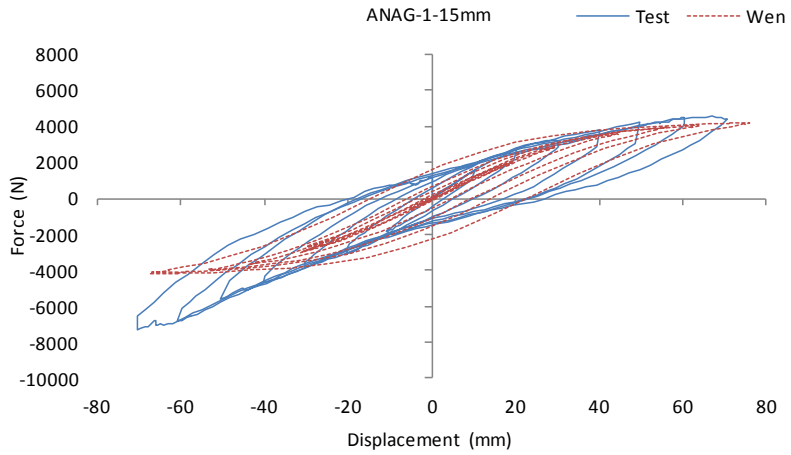

Figure 33. Comparison of the hysteretic cycles of the experimental test with those of the Bouc-Wen model for the ANAG-1-15mm device.

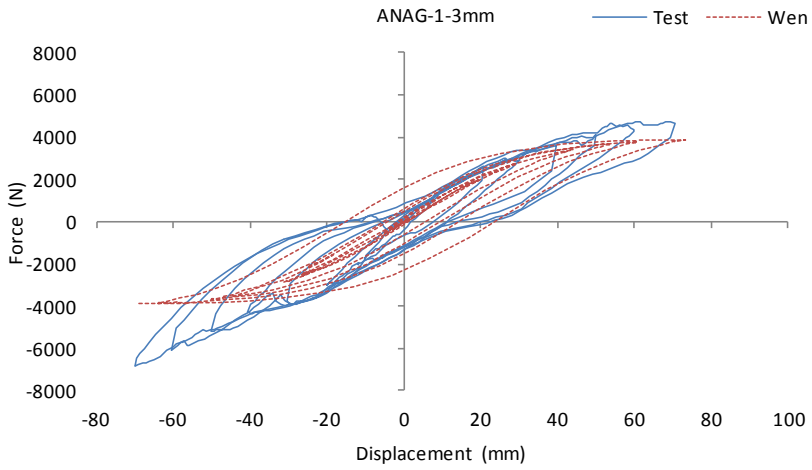

Figure 34. Comparison of the hysteretic cycles of the experimental test with those of the Bouc-Wen model for the ANAG-1-3mm device.

*Corresponding Author:Gustavo Gioacchini67 | Page
National Technological University, Mendoza Regional Faculty, CeReDeTeC

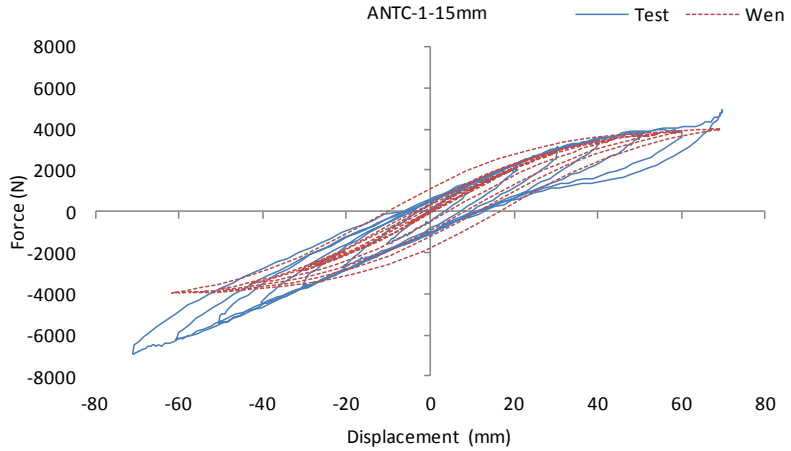

Figure 35. Comparison of the hysteretic cycles of the experimental test with those of the Bouc-Wen model for the ANTC-1-15mm device.

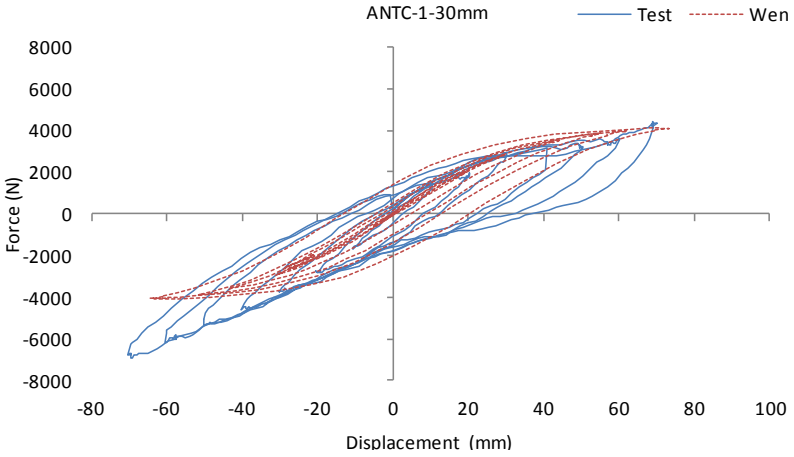

Figure 36. Comparison of the hysteretic cycles of the experimental test with those of the Bouc-Wen model for the ANTC-1-30mm device.

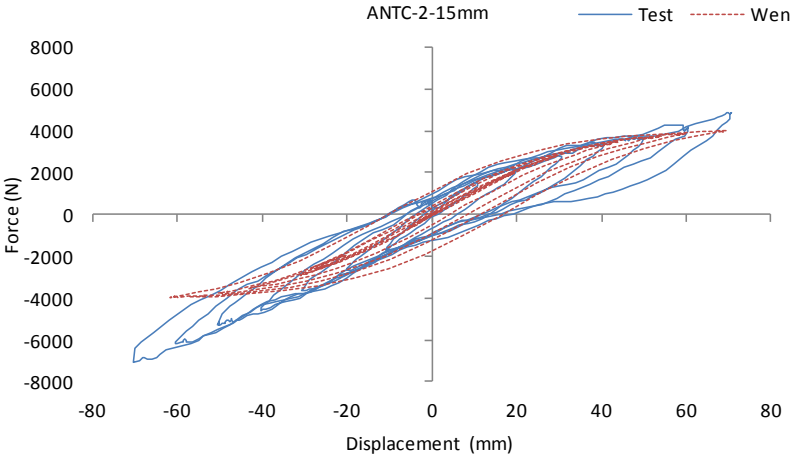

Figure 37. Comparison of the hysteretic cycles of the experimental test with those of the Bouc-Wen model for the ANAF-1-15mm device.

In order to assess the degree of accuracy, a quantitative comparative analysis has been carried out. From the hysteretic cycles generated from the Bouc-Wen model, the theoretical effective rigidity and damping is determined [21]. The procedure for one of the cases studied is described below. Figure 38 shows the envelope of the hysteretic cycle area of the Wen model for the ASNC-1-15mm device.

*Corresponding Author:Gustavo Gioacchini68 | Page
National Technological University, Mendoza Regional Faculty, CeReDeTeC

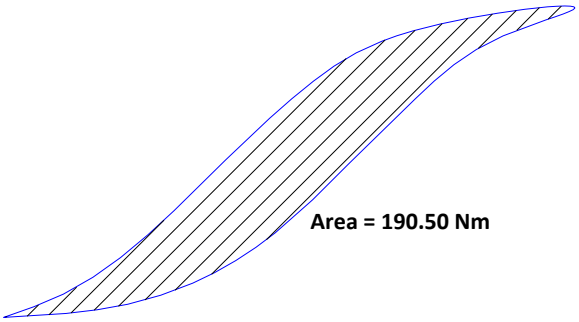

Figure 38. Hysteretic cycle area of the Wen model for the ASNC-1-15mm device.

Effective rigidity: $K_{eff} = \frac{|F^+| + |F^-|}{|\Delta^+| + |\Delta^-|} = 59{,}42\ N/mm$

F^+= 3.714 NΔ^+= 66 mmF^-= -3714 NΔ^-= -59 mm

Wo= Hysteretic cycle area = 190.500 Nmm

Elastic energy: $w_e = \frac{1}{2} K_{eff}\, \delta^2 = 129.430 Nmm$

Effective damping: $\xi_{eff} = \frac{w_0}{4\ \pi\ w_e} = \frac{190.500 Nmm}{4\ \pi\ 129.430 Nmm} = 0{,}117 = 11{,}70\%$

Table 7 summarizes the effective damping obtained from the tests (*keff*) and those obtained with the Bouc-Wen model (*kefft*). The results indicate that the parameters of the Wen model adequately represent the hysteretic cycle area and effective damping but they do not adequately represent the post-creep rigidity (Figures 31 to 37).

Where *Wo* is the area of the hysteretic cycle; *F+ y F-* are the maximum and minimum forces obtained from the hysteretic cycle; *Δ+ y Δ-* are the maximum and minimum displacements obtained from the hysteretic cycle; *keff* is the effective rigidityand*We* is the elastic energy. The values correspond to those obtained from the tests. Those which have to correspond to Wen model.

Table 8 shows the effective stiffness obtained from the experimental tests. The effect of the asymmetry and the rigidities of Wen model have been neglected. The results indicate that in six out of the eight cases studied, the differences are less than 20%.

Table 7. Comparison of the effective damping obtained from the tests *(ξeff)*with that, obtained with the Bouc-Wen model*(ξ_{efft})*.

Parameter	Unit	PROTOTYPES OF ISOLATORS										
		ASNC-1		ASNC-2		ANAG-1		ANAG-2	ANTC-1		ANTC-2	ANAF-1
		15 mm	30mm	15 mm	30mm	15 mm	3mm	15 mm	15 mm	30mm	15 mm	15 mm
W_o	Nmm	220210	400130	315590	442020	406180	361330	588490	261480	395290	327500	434650
F^+	N	3709	4000	5481	4759	4554	4736	5923	4926	4365	4863	5901
F^-	N	6808	6865	7236	7616	7348	6836	6665	6928	6793	7104	9730
Δ^+	Mm	60,00	70,00	71,00	70,00	70,00	71,00	71,00	70,00	70,00	71,00	70,00
Δ^-	Mm	60,00	71,00	70,00	70,00	70,00	70,00	70,00	71,00	70,00	70,00	70,00
k_{eff}	N/mm	87,64	77,06	90,19	88,39	85,01	82,07	89,28	84,07	79,70	84,87	111,65
W_e	Nmm	157755	188789	227328	216563	208285	206860	225022	205974	195265	213921	273543
ξ_{eff}	%	11,1	16,9	11,0	16,2	15,5	13,9	20,8	10,1	16,1	12,2	12,6
$W_{o\,t}$	Nmm	190500	357300	220860	333500	331440	268320	444890	193960	317140	214960	309190
F^+_t	N	3714	4183	4219	4050	4186	3899	4158	4001	4119	4001	4633
F^-_t	N	3714	4183	4181	4059	4183	3910	4171	3958	4072	3956	4586

*Corresponding Author:Gustavo Gioacchini69 | Page
National Technological University, Mendoza Regional Faculty, CeReDeTeC

Table 7. Comparison of the effective damping obtained from the tests *(ξeff)*with that, obtained with the Bouc-Wen model*(ξ_{efft})(Continuation).*

Parameter	Unit	PROTOTYPES OF ISOLATORS										
		ASNC-1		ASNC-2		ANAG-1		ANAG-2	ANTC-1		ANTC-2	ANAF-1
		15 mm	30mm	15 mm	30mm	15 mm	3mm	15 mm	15 mm	30mm	15 mm	15 mm
Δ^+_t	Mm	66,00	76,00	70,00	76,00	76,00	73,00	79,00	69,00	73,00	69,00	83,00
Δ^-_t	Mm	59,00	67,00	64,00	71,00	67,00	69,00	77,00	62,00	64,00	62,00	73,00
$k_{eff\,t}$	N/mm	59,42	58,50	62,69	55,16	58,52	54,99	53,39	60,76	59,79	60,74	59,10
$W_{e\,t}$	Nmm	129425	168958	153582	159312	169019	146529	166607	144629	159306	144593	203557
$\xi_{eff\,t}$	%	11,7	16,8	11,4	16,7	15,6	14,6	21,2	10,7	15,8	11,8	12,1

Table 8. Comparison of the effective rigidity obtained from the tests (*keff*) with that obtained from the Bouc-Wen model (*kefft*)

Parameter	Unit	PROTOTYPES OF ISOLATORS										
		ASNC-1		ASNC-2		ANAG-1		ANAG-2	ANTC-1		ANTC-2	ANAF-1
		15 mm	30mm	15 mm	30mm	15 mm	3mm	15 mm	15 mm	30mm	15 mm	15 mm
F^+	N	3709	4000	5481	4759	4554	4736	5923	4926	4365	4863	5901
F^-	N	3709	4000	5481	4759	4554	4736	5923	4926	4365	4863	5901
k_{eff}	N/mm	61,82	56,74	77,74	67,99	65,06	67,18	84,01	69,87	62,36	68,98	84,30
F^+_t	N	3714	4183	4219	4050	4186	3899	4158	4001	4119	4001	4633
F^-_t	N	3714	4183	4181	4059	4183	3910	4171	3958	4072	3956	4586
$k_{eff\,t}$	N/mm	59,42	58,50	62,69	55,16	58,52	54,99	53,39	60,76	59,79	60,74	59,10
e	%	3,87	3,02	19,37	18,86	10,04	18,14	36,45	13,05	4,12	11,94	29,90

4.3. HYPERELASTICMODELOGDENSIMULATION

For the numerical modeling of the device, the commercial Abaqus code has been used [16]. In this paper we present only the results for the prototype ASNC.The model represents the experimental test for a vertical displacement of 30 mm and seven cycles of horizontal displacements of +/- 10 mm, 20 mm, 30 mm, 40 mm, 50 mm, 60 mm and 70 mm.In the finite element model (MEF), the global displacements have been restricted in three directions, the lower part of the isolation, in coincidence with the lower connection plate, theoretically in contact with the foundation structure. Figure 39 shows the MEF of the device.

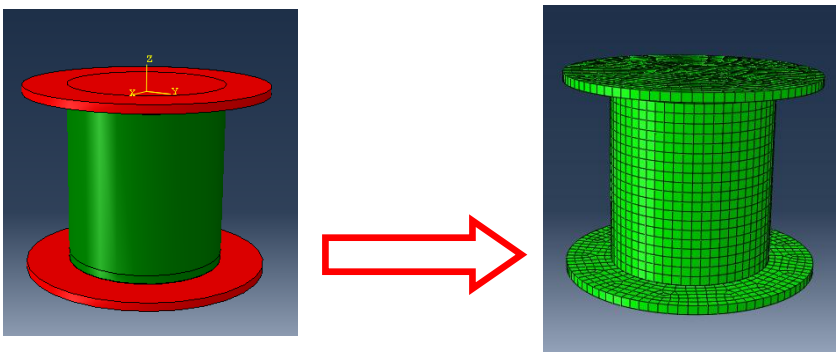

Figure 39. Finite element model of the device [16].

Figure 40 shows the model of the device under vertical load and controlled vertical deformation. The responses obtained with the Ogden hyper elastic model are compared to the results obtained experimentally. Figure 40 shows the similarity of response between the model and the tests.

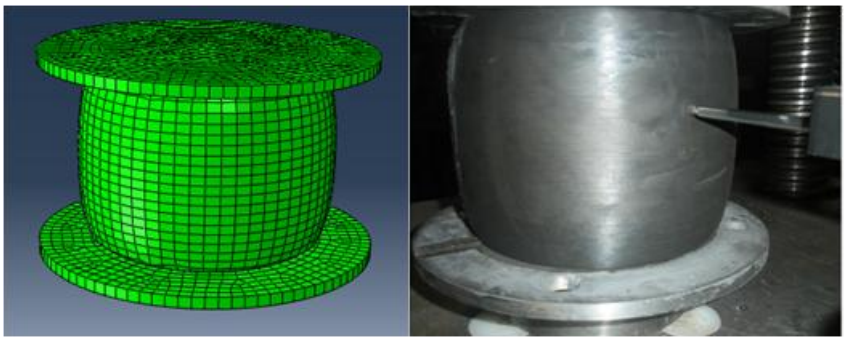

Figure 40. Comparison of the response to vertical load of compression for the MEF and theexperimental test.

4.3.1. OGDEN MODELPARAMETERS

The materials used for the modeling were rubber and steel. For the steel, an isotropic elastic model with an elastic module E = 210000 MPa was used. For the elastomer, the Ogden hyper elastic model was used [22]. The parameters corresponding to the Ogden model have been obtained experimentally and simultaneously by traction, compression and cutting tests, which are summarized in Table 9 [23]. A value of k = 10000 MPa has been used for the volumetric module. If that value is used, the numerical results describe a practically incomprehensible response.

Table 9. Parameters corresponding to the Ogden model.

Constants (MPa)						
Compound	μ_1	μ_2	μ_3	α_1	α_2	α_3
Rubber	10	0,012	-0,1	1,3	5	-2

4.3.2. HYPERELASTICMODEL OF SIMULATION THEELASTOMER.

The constitutive model used to simulate the behavior of the elastomer is based on the energy function proposed by Ogden [22] [24] [25].

$$W(\lambda_1,\lambda_2,\lambda_3)=\sum_{i=1}^{N}\frac{\mu_i}{\alpha_i}(\lambda_1^{\alpha_i}+\lambda_2^{\alpha_{i_i}}+\lambda_3^{\alpha_i}-3) \quad \rightarrow 10$$

Where N is a positive whole number andμ_i, $\alpha_i$are parameters of the material that are determined based on experimentaltests [23]. The deformations are parameterized by the main stretches λ_A given by the following expression:

$$\lambda_A=(eig_A(C))^{1/2}=(eig_A(B))^{1/2} \quad \rightarrow 11$$

Where the eigenvalues are obtained as from the right tensor of Cauchy-Green C or the left tensor of Cauchy-Green$B$. Due to the quasi-incomprehensibility presented by the elastomers, a multiplicative decomposition of the gradient tensor of deformation is carried out in its volumetric parts ($Fvol$) and diverter(F).

4.3.3. RESULTS OF THEHYPERELASTICMODEL

The relationshipforce-displacement has been determined (Figure 41). Figure 42 shows the relationshipforce-displacement superimposed of the MEF and that obtained from the experimental test. It is observed that both hysteretic cycles present a good qualitative approximation.The maximum and minimum forces and displacements of the MEF are similar to those obtained in the experimental tests. It´s important to take into account that the hysteretic cycles of the tests do not present symmetries, while the one achieved as from the numerical model is symmetric in its hysteretic development.

*Corresponding Author:Gustavo Gioacchini71 | Page
National Technological University, Mendoza Regional Faculty, CeReDeTeC

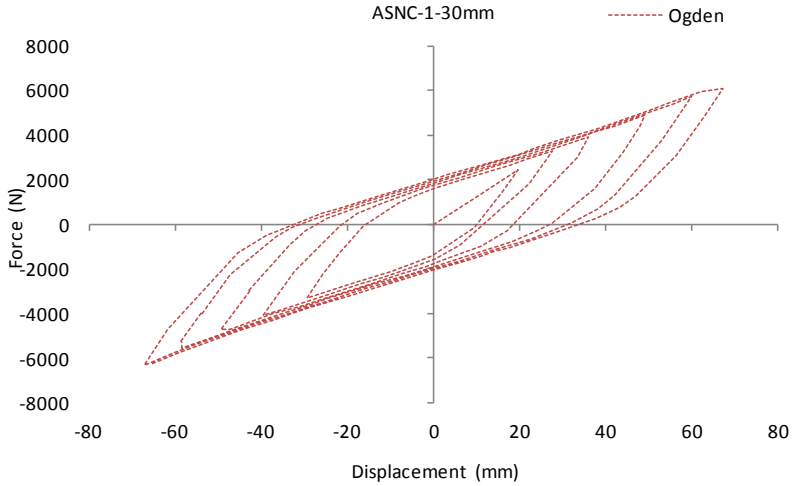

Figure 41. Hysteretic cycle of the Ogden numerical model in Abaqus for the ASNC-1-30mm device.

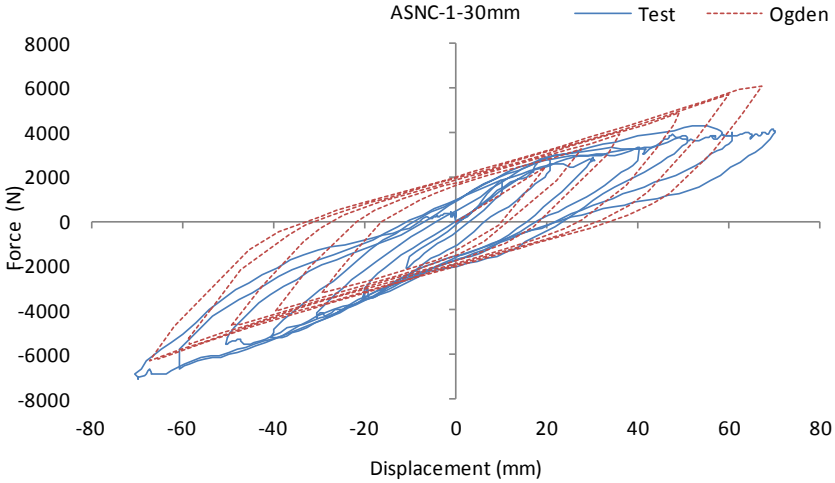

Figure 42. Comparison of the hysteretic cycles of the experimental test with the Ogden model for the ASNC-1-30mm isolation.

Figures 43, 44 and 45 show the distribution of axial and cutting stresses S11, S33 and S12, for the Ogden hyper elastic model and for the maximum external actions which are reproduced from the experimental test and Figure 46 shows the correspondence, in terms of deformations, between the experimental test and the Ogden numerical model.

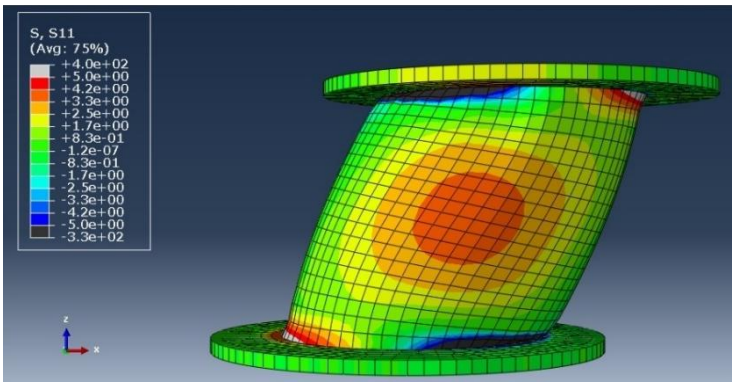

Figure 43. Axial stress state S11 for the x axis [MPa x e-01].

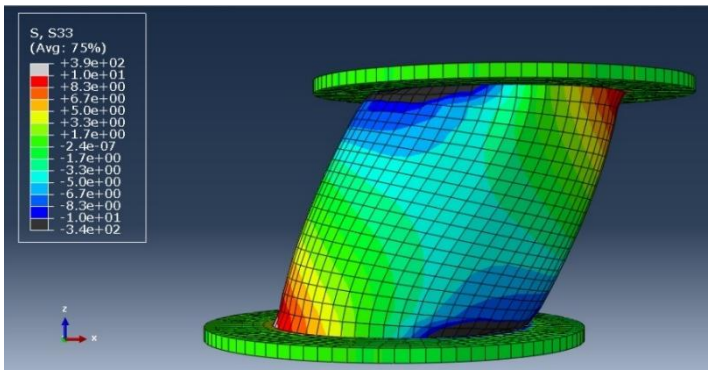

Figure 44. Axial stress state S33 for the z axis [MPa x e-01].

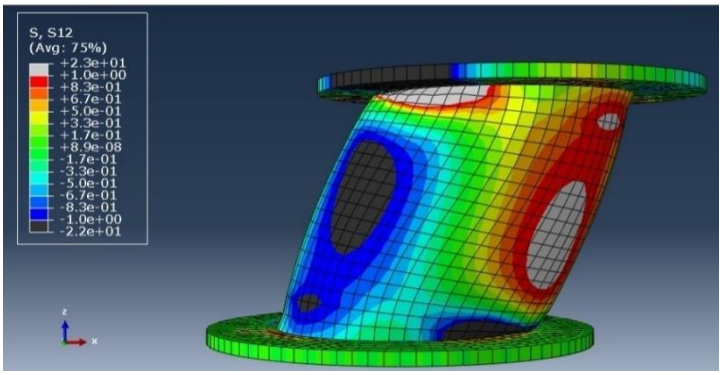

Figure 45. Shear stress state S12 for the x-y axes [MPa x e-01].

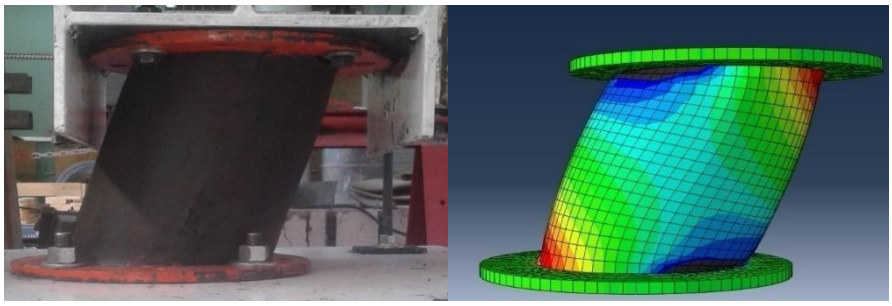

Figure 46. Qualitative comparison of the response obtained in the experimental test and the Ogden numerical model.

The maximum stresses are found in the union of the upper and lower connection steel plates with the rubber of the device. The axial stress for the x axis (S11) (Figure 49) decreases from the core of the rubber to the outside. Figure 44 shows that the axial stress for the *z* axis (S33) presents diagonal symmetry in its distribution with maximum values in its extremes. The cutting stress S12 (Figure 45) shows a symmetric distribution, with concentration of stress at different points of the isolation.

In order to perform a quantitative comparative analysis, the effective rigidity and damping of the Ogden numerical model and the experimental tests are determined. The procedure used is the same as that used for the Wen model, that is, to quantify the energy dissipated by the isolation and the effective damping [21] because the two parameters are of interest to evaluate the responses of structures with seismicisolation.

Figure 47shows the surrounding of the hysteretic cycle area for the Ogden numerical model of the prototype ASNC-1-30m (envelope the hysteresis cycles of Figure 19).

*Corresponding Author:Gustavo Gioacchini73 | Page
National Technological University, Mendoza Regional Faculty, CeReDeTeC

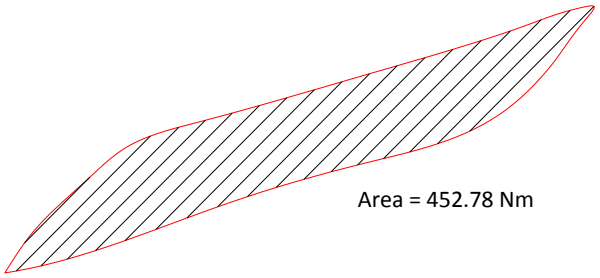

Figure 47. Hysteretic cycle area obtained from the Ogden model for the prototype ASNC-1-30mm.

Effective rigidity: $K_{eff} = \frac{|F^+| + |F^-|}{|\Delta^+| + |\Delta^-|} = 92{,}29 \, N/mm$

F^+= 6.067 NΔ^+= 67 mmF^-= -6308 NΔ^-= -67 mm

Wo= Hysteretic cycle area = 452.780 Nmm

Elastic energy: $w_e = \frac{1}{2} K_{eff} \delta^2 = 207.396 Nmm$

Effective damping: $\xi_{eff} = \frac{w_0}{4 \pi w_e} = \frac{452.780 Nmm}{4 \pi 207.396 Nmm} = 0{,}174 = 17{,}40\%$

Table 10 summarizes the effective damping obtained from the test and that obtained with the Ogden numerical model.

Table 10. Comparison of the effective damping obtained from the test and the numerical model of Ogden in Abaqus.

Parameter	Units	PROTOTYPE OF ISOLATOR	
		ASNC-1-30mm	
		Experimental Test	Ogden'sHyperelastic
W_o	Nmm	400130	452780
F^+	N	4.000	6.067
F^-	N	6.865	6.308
Δ^+	Mm	70,00	67,04
Δ^-	Mm	71,00	67,04
k_{eff}	N/mm	77,06	92,29
W_e	Nmm	188.789	207.396
ξ_{eff}	%	16,9	17,4

The results obtained allow us to conclude that the Ogden numerical model is acceptable to represent the experimental tests of the ASNC devices.

V. CONCLUSIONS

The physical and mechanical tests allowed to verify the quality of the manufacture of the devices and their materials.

For tests on vertical and horizontal cyclic loads, the maximum horizontal displacements have been reached without any type of failure in the devices.

When the vertical displacement increases, as a consequence of a greater compression load, the horizontal force-displacements curves, enclose larger areas and therefore there is a greater dissipation of energy.

The effective horizontal rigidity of the devices does not present significant degradation when the vertical load and the horizontal force are increased. The effective rigidity of the isolation remains almost constant throughout the entire test and for the levels of imposed loads.

*Corresponding Author:Gustavo Gioacchini74 | Page
National Technological University, Mendoza Regional Faculty, CeReDeTeC

The effective damping determined with the experimental tests reach acceptable values (10% to 20%) and similar to other elastomeric isolation that arecommercialized in the market.

The evaluation of the Bouc-Wen model has been made by comparing the effective damping obtained from the tests (*keff*) with those obtained from (*kefft*). The results indicate that the numerical model allows to represent the response of the isolation in terms of area of the hysteretic cycle and effective damping. The model does not adequately represent the post-creep rigidity.

The evaluation of the Ogden model has been made by comparing the energy dissipated by the isolation and its effective damping. The results indicate that the numerical model Ogden is suitable to represent the experimental tests of the ASNC devices.

ACKNOWLEGEMENTS

The work has been developed within the Research Project UTI4335TC of the UTN. The authors thank the authorities of CeReDeTeCand the Mendoza Regional Faculty of the National Technological University, for the support given in the development of the work.

REFERENCES

[1]. EM-DAT. The OFDA/CRED International Disaster Database - www.emdat.be. Bruselas: UniversitéCatholique de Louvain. 2011.
[2]. Kelly J. M. and Marsico M. R. Stability and post-buckling behavior in nonbolted elastomeric isolators. Mathematical sciences publishers. 2010. Vol 1- nº1.
[3]. Besa, J., de la Llera J. C., Jünemann R. Experimental behavior and design of a new kinematic isolator. EngineeringStructures. 2010. Vol.32, 508-522.
[4]. Revista BIT, Especial terremoto Chile 2010. Aislación y disipación de energía. Mayo 2010. (Disponible online www.fiic.la/lxv consejo directivo panama/delallera 2.pdf.), 2010.
[5]. Auqui M. V., Aguiar R., Gómez P. Análisis de aisladores sísmicos elastoméricos construidos en Ecuador. Proyecto previo a la obtención de título de ingeniero civil. 2010.
[6]. Aguiar R., Almazán J. L., Dechent P., Suárez V. Aisladores de base Elastoméricos y FPS, Centro de Investigaciones Científicas. Escuela Politécnica del Ejército, Quito, Ecuador. 2008. 292 p.
[7]. Donà M., Muhr A. H., Tecchio G. and Porto F. Experimental characterization, design and modelling of the RBRL seismic-isolationsystemforlightweightstructures. EarthquakeEngineering&Structural Dynamics. 2017. Vol 46 – Issue 5 - Pages 831-853
[8]. Araya Acle L. M., Moroni O. M., Sarrazin A. M., Jorquera P. Desarrollo y fabricación de aisladores sísmicos para edificio habitacional. Universidad de Chile. Facultad de Ciencias Físicas y Matemáticas. Departamento de Ingeniería Civil. Memoria para optar el título de Ingeniero Civil. Santiago Chile. 1994.
[9]. Gioacchini G., Tornello M., Frau C. Cuantificación de los parámetros elásticos y mecánicos de un nuevo dispositivo de aislamiento sísmico. Revista Internacional de Ingeniería de Estructuras. Editores: Alex H. Barbat, Roberto Aguiar. ISSN 1390-1117. 2015. Vol. 20,2, 199 - 212.
[10]. IRAM 113003. Elastómeros y plastómeros. Método de determinación de la dureza Shore A y Shore D. 1989.
[11]. ASTM D2240 - 05. Standard Test Method for Rubber Property - Hardness tester Hardness 2010.
[12]. ASTM D412 – 06a. Standard Test Methods for Vulcanized Rubber and Thermoplastic Elastomers – Tension. 2013.
[13]. ASTM D395 - 14. Standard Test Methods for Rubber Property—Compression Set. 2014.
[14]. Kelly, J. M. Earthquake-Resistant Design with Rubber. Springer – Verlag. London. 1993, 1996 2nd edition.
[15]. MatLab version 7.10.0. Natick, Massachusetts: The MathWorks Inc. 2010.
[16]. Abaqus 6.4-1. Theory Manual. Hibbit, Karlson and Sorenson, Inc.: Pawtucket, U.S.A. 2003.
[17]. Bozzo, L. Análisis de edificios con sistemas de aislamiento de base. En: Barbat, A.; L. Aguiar, eds. Ingeniería de estructuras. Escuela superior politécnica del ejército. Quito, Ecuador. 1996. 1(1): 17-38
[18]. Ordoñez, D. Estudio comparativo de la respuesta estructural inelástica de edificios sismorresistente con aislamiento de base. Tesis Mag. Ing. Sísmico y Dinámica Estructural. Universidad Politécnica de Cataluña. 1996. 58p.
[19]. Wen, Y. Method for random vibration of hysteretic system. Journal of the engineering mechanics division. 1976. 102 (EM2):249-26.
[20]. Wilson E. L. 3º Edición. Three – dimensional static and dynamic analysis structures. Computers and Structures, Inc. Berkeley, California, USA. 2002.
[21] Tornello M. Aislamiento sísmico de base en construcciones civiles, emplazadas en zonas de alto riesgo sísmico. Director: Dr. Sarrazin A. M. Tesis Doctoral. Universidad Tecnológica Nacional – Facultad Regional Mendoza. 2007.
[22]. Ogden R. Non-linear elastic deformations, Dover Publications, New York. 1984.
[23] Weinberg K. Lecture Notes for ZurMethodFinitenElemente in der Mechanik II: NichtlineareProbleme, TU Berlin [in English].http://mechanik.tu berlin.de/weinberg/Lehre/fem2/Chapter4.pdf.2010.
[24] Núñez C. A. y Celentano D. J. Caracterización experimental y numérica de compuestos elastoméricos utilizados en disipadores de energía. Mecánica Computacional Vol. XXIV A. Larreteguy (Editor) Buenos Aires, Argentina. 2005.
[25] Bellomo F., Nallim G., Oller S. Modelo para el análisis del comportamiento mecánico de materiales compuestos de matriz elastomérica reforzada. Mecánica Computacional Vol XXVII. Alberto Cardona, Mario Storti, Carlos Zuppa. (Eds.) San Luis, Argentina. 2008. pág. 593-613.

Gustavo Gioacchini " Design, manufacture and simulation of Seismic Isolation Device for a Low Level Axial Load" Quest Journals Journal of Research in Humanities and Social Science , vol. 04, no. 01, 2019, pp. 50-75

*Corresponding Author:Gustavo Gioacchini75 | Page
National Technological University, Mendoza Regional Faculty, CeReDeTeC